Early Age Cracking Control in Semimassive Walls of RC Tanks by Internal Cooling

Mariusz Zych[1] and Trong-Chuc Nguyen, Ph.D.[2]

Abstract: Semimassive tanks must satisfy the requirement of watertightness, so all attempts to reduce early-age imposed strains lead to considerable financial savings. The impact of a cooling pipe system (CPS) on a reinforced concrete (RC) tank wall where early-age cracks developed during construction has been analyzed. It has been proven that for RC tanks, the factor that contributes most to tensile stresses in the semimassive walls is the mean temperature of the maturing concrete. The second most influential factor is derived from self-stresses, and the least influential factor is the stress gradient. The calculations of self-stresses indicate that the use of a CPS leads to the formation of favorable compressive rather than tensile stresses in the central part of the wall. Most importantly, a CPS in RC tank walls significantly reduces the width of cracks that result from the cumulative effect of early-age and long-term imposed strains. The performed analysis provides a basis for the effective design of a CPS in RC tank semimassive walls. **DOI: 10.1061/(ASCE)CF.1943-5509.0001585.**

Author keywords: Cracks; Concrete construction; Reinforced concrete (RC) tank; Hydration age; Cooling pipe system (CPS).

Introduction

Due to the periodic but significant accumulation of the heat of hydration, semimassive and massive reinforced-concrete (RC) structures are subject to significant temperature changes in the most intense cement hydration period. A practical way to determine the degree of the massiveness of a structural element is based on determining the surface-area-to-volume ratio (subsequently referred to as surface moduli). According to the definition, the surface moduli $m_c = u_c/v_c$ (Flaga 2004), where u_c is the surface area of an element that is exposed to air and v_c is the volume of the element. The semimassive elements are defined as those for which $2\ \mathrm{m}^{-1} < m_c < 15\ \mathrm{m}^{-1}$. The restrained parts of imposed strains generate both self-stresses (the influence of internal restraints) and stresses that result from the occurrence of external restraints (Knoppik-Wróbel 2015). This phenomenon results in tensile stresses, which often cause the formation of through-cracks. For some structures, these cracks are of key importance in satisfying the serviceability limit state and durability of the structure. A typical example of such structures is RC tanks, which must be watertight, i.e., the width of the cracks must be limited to 0.1 mm. The state-of-the-art knowledge of thermal cracking of massive structures was presented in a collective work published under the auspices of Rilem by Fairbairn and Azenha (2019).

For massive structures, one of the most effective methods to reduce unwanted strains of curing concrete is to use internal cooling. As described by Nguyen et al. (2019), its main task is to reduce the temperature differences between the interior of the member and its outer surface. In massive concrete structures, such as dams and bridge foundations, thermal cracks are often observed during hydration, especially in the early stages of strength formation (Kogan 1980). When a cooling pipe system (CPS) is used, the water flow absorbs heat from the concrete and removes heat to the outside during hydration, as presented by Hauser et al. (2000). In this method, the maximum temperature in concrete blocks and the temperature difference between the core and surface of the concrete block are reduced. The risk of crack formation is also greatly reduced. The cooling pipe system was first employed in the construction of the Hoover Dam in 1933 (Chen et al. (2011). Other examples of the application of a pipe cooling system include the Xiang Hong Dian Dam in China in 1955, the Bureyskaya hydroelectric power plant in Russia in 1978, the Seo-He Bridge in Korea in 2000, the Tuyen Quang Dam in Vietnam in 2002, and the Dagangshan Dam in China in 2013, as quoted by Nguyen and Aniskin (2019), Li and Li (2017), and Liu et al. (2015).

The main objective of using a CPS in massive structures is to lower the maximum temperature inside the structure to reduce the temperature difference between the interior and the surface layers (Bofang 2014). The application of the internal cooling technology has proven effective in massive structures (i.e., structures that satisfy the condition, $2\ \mathrm{m}^{-1} \geq m_c$), but its employment in the walls of semimassive tanks (i.e., structures that satisfy the condition, $2\ \mathrm{m}^{-1} < m_c < 15\ \mathrm{m}^{-1}$) has not been analyzed. The first part of the presented analysis exemplified by a semimassive structure provides information on the beneficial effect of CPS and the scope of this effect on changes in individual temperature components, i.e., average temperature, temperature gradient, and temperature causing self-stresses. The specificity of semimassive structures (Jędrzejewska et al. 2020), as opposed to massive structures (Kanavaris et al. 2021), is a different way of cracking, which results, for example, from the different domination of external and internal restraints (Bamforth 2018) and thus from the different weight of the importance of the aforementioned individual temperature components. Early-age cracking models dedicated to semimassive structures [i.e., the restraint of a member at its ends or

[1]Ph.D. Civil Engineering Associate Professor, Institute of Building Materials and Structures, Dept. of Civil Engineering, Cracow Univ. of Technology, St. Warszawska 24, Kraków 31-155, Poland (corresponding author). ORCID: https://orcid.org/0000-0002-1890-9891. Email: mzych@pk.edu.pl

[2]Institute of Techniques for Special Engineering, Le Quy Don Technical Univ., No. 236, Hoang Quoc Viet St., Bac Tu Liem Dist., Hanoi City 1000, Vietnam. Email: ntchuc.mta198@gmail.com

Note. This manuscript was submitted on July 28, 2020; approved on December 29, 2020; published online on April 20, 2021. Discussion period open until September 20, 2021; separate discussions must be submitted for individual papers. This paper is part of the ***Journal of Performance of Constructed Facilities***, © ASCE, ISSN 0887-3828.

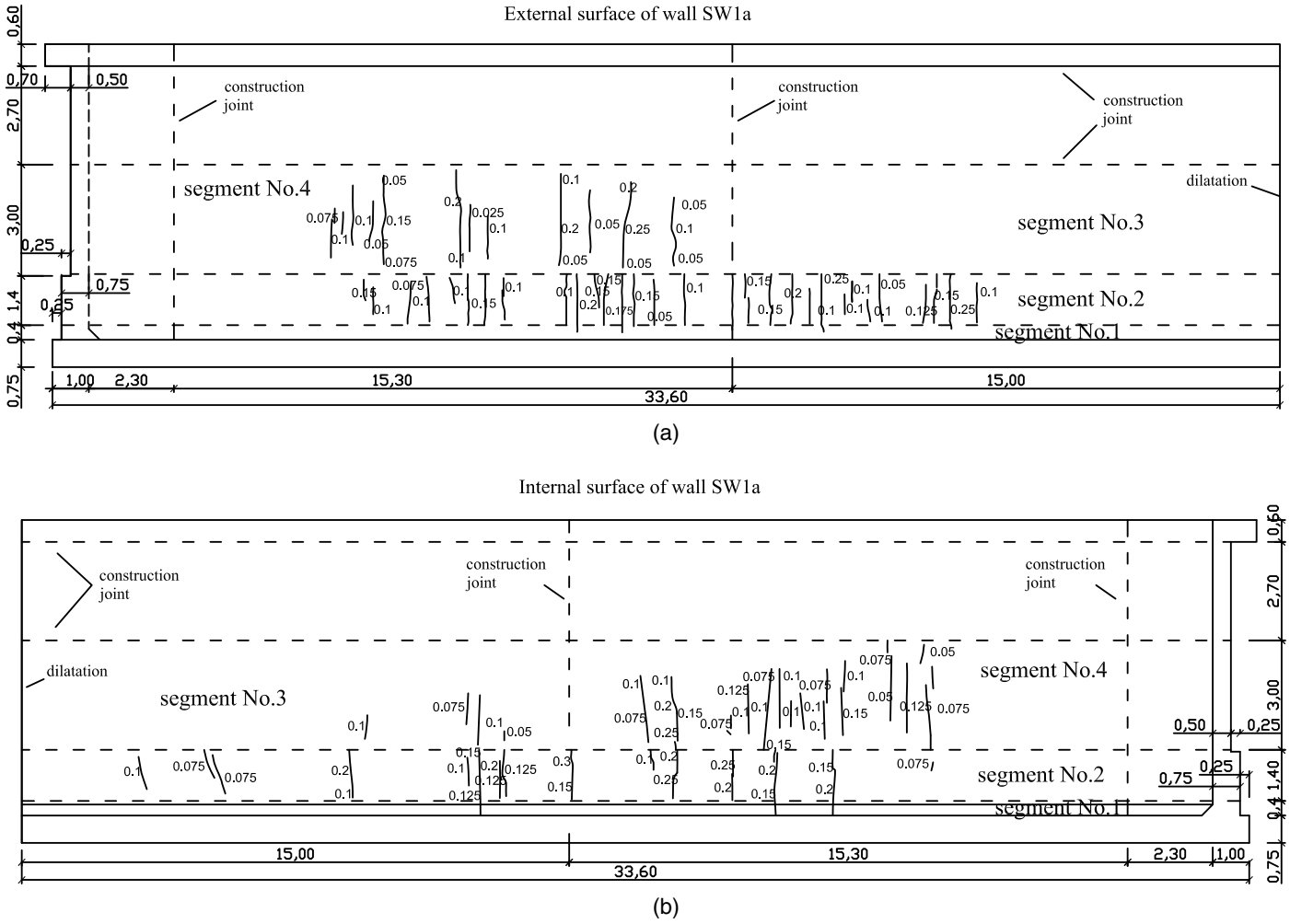

Fig. 1. Layout of cracks and their widths on the (a) outside; and (b) inside wall surfaces. (Adapted from Zych 2008.)

the restraint along with one-edge models in Eurocode 2 (CEN 2006)] cannot be used in the analysis of massive structures. Therefore, together with the second part of the analysis, which consists of assessing the influence of the CPS on avoiding early-age cracking or reducing it, this paper presents a new practical tool for the design of semimassive structures, such as tank walls, bridge abutments, or tunnel walls (Jędrzejewska et al. 2020). Therefore, the proposed solution for a semimassive structure is innovative, and all results presented in this paper in relation to this structure constitute a novelty in the current state of knowledge. The present paper aims to perform an analysis of the impact of this technology in a semimassive RC tank wall ($m_c = 2,7$), where early-age cracking developed during its construction. A question arises: what is the effectiveness of this solution, and what effects of internal cooling should be expected? In the paper, based on the numerical model (Nguyen and Aniskin 2019) for massive structures, the internal cooling technology to minimize imposed strains generated by the development of the heat of hydration was analyzed by using a semimassive tank wall as an example.

Structure Geometry and Materials Properties

A computational analysis was performed on a wall of a rectangular reinforced concrete tank with a nominal unit capacity of 30,000 m^3. The walls were sequentially concreted and monolithically joined to the bottom slab, which is the basic member that restrains the imposed strains in successively concreted walls. According to the classification of massiveness of the structure (Flaga 2004), the walls of this tank were classified as semimassive.

An external wall denoted as SW1a was selected for the analysis. This wall was analyzed using FEM by Zych (2008) with regard only to its early-age cracking without internal cooling. The SW1a wall was constructed in stages, i.e., by executing subsequent segments (Fig. 1). The basic mechanical properties of concrete were tested (Table 1). Thermophysical properties, i.e., the coefficients of thermal conductivity and specific heat capacity, were determined based on the composition of the concrete mix, as proposed by Rostásy and Krauß (2003), Aleksandrovski (1966), Van Breugel (1996), and Hamfler (1988). The thermophysical properties of

Table 1. Tested mechanical concrete properties

Concrete age (days)	f_{cm} (MPa)	$E_{cm0,4}$ (GPa)	f_{ctm} (MPa)
2	10.10	14.10	1.12
3	14.86	17.29	1.32
4	19.06	17.82	—
7	22.24	19.91	1.54
28	30.89	22.53	1.86

Source: Data from Seruga and Zych (2015).

Table 2. Thermophysical characteristics of the concrete mass and soil

Thermophysical characteristics	Concrete		Soil
	Segment wall no. 2 (young concrete)	Foundation slab (old concrete)	Gravel ground (natural humidity)
Thermal conductivity (W/m · °C)	2.59	2.16	1.3
Specific heat capacity (J/kg · °C)	965	772	800
Density (kg/m^3)	2,240	2,240	1,800
Surface heat transfer coefficient (W/m^2 · °C)			
Boundary 1 (free contact with air)	21.60	21.60	—
Boundary 2 (formwork)	5.20	—	—
Thermal expansion coefficient (1/°C)	1.1×10^{-5}	1.1×10^{-5}	1.0×10^{-5}

the soil were determined as proposed by Voigt (1994). The thermophysical properties of the concrete wall, slab foundation, and soil used in the analysis are presented in Table 2.

Numerical Model

The temperature field in a mass concrete structure with the CPS is determined by solving two differential Fourier equations by following the principle of energy balance and is described by Myers et al. (2009), Hong et al. (2017), and Qiu and Zhang (2017). One differential Fourier equation is the basic equation of the theory of thermal conductivity considering the release of heat due to cement hydration

$$k_c \nabla^2 T_c + Q_h = \rho_c c_c \frac{\partial T_c}{\partial t} \tag{1}$$

where T_c = temperature of concrete at age t days (°C); k_c = thermal conductivity of concrete (W/m · °C); Q_h = heat of hydration (W/m^3); c_c = specific heat of concrete (kJ/kg · °C); ρ_c = mass density of concrete (kg/m^3); and t = time (day).

The other equation includes the heat exchange between the pipe cooling system and concrete

$$\rho_w c_w \left(\frac{\partial T_w}{\partial t} + \vec{u} \nabla T_w \right) = k_w \nabla^2 T_w \tag{2}$$

where T_w = temperature of water at age t days (°C); k_w = thermal conductivity of water, (W/m · °C); c_w = specific heat of water (kJ/kg · °C); ρ_w = mass density of water (kg/m^3); and $\vec{u}$ = vector of the water flow in the pipe.

Fourier Eqs. (1) and (2) can be solved using the initial boundary conditions and a given graph of the cement heat release during the hydration of cement (Myers et al. 2009)

$$T_{ini}(x, y, z, 0) = T_0(x, y, z) = \text{const.} \tag{3}$$

where $T_{ini}(x, y, z, 0)$ = initial temperature of the concrete.

The temperature change in concrete due to the heat released during the hydration process largely depends on the environment and boundary conditions. Furthermore, phenomena such as conduction, convection, solar radiation, and radiation simultaneously occur and increase the analysis complexity.

Convection is expressed by Newton's law of cooling, which states that the rate of heat loss of a body is proportional to the difference between its own temperature and its surroundings. The convection boundary condition is expressed as Eq. (4), as presented by Nguyen and Aniskin (2019)

$$q_{\text{conv}} = h_c (T_c - T_{\text{amb}}) \tag{4}$$

where T_c = temperature of a body; h_c = convection coefficient (also called the film coefficient), which mainly depends on the surface texture and velocity of the ambient air; and T_{amb} = ambient temperature.

The principle of heat transfer through the cooling tube is that the heat is transferred from concrete to the cooling pipe through the pipe wall and mainly within the cooling pipe. To determine the pipe temperature, the pipe arrangement is assumed to consist of several pipe parts connected with one another. Each pipe is assumed to have a length perpendicular to the calculation plane. The inlet temperature of each tube is T_{inlet}, and either the outlet temperature T_{outlet} or pipe flow q must be specified. The approximate heat is removed from the concrete using CPS, as shown by Eq. (5)

$$Q_p = \sum_{i=1}^{n} q_i l \tag{5}$$

where q_i = heat energy transferred through pipe part i.

Using thermal equilibrium, if the pipe outlet temperature is specified, the energy required to arrange the cooling pipe system is determined as Eq. (6)

$$q = \frac{Q_p}{c_w (T_{\text{outlet}} - T_{\text{inlet}})} \tag{6}$$

If the heat energy that must be removed from concrete is specified, the outlet temperature is determined by Eq. (7)

$$T_{\text{outlet}} = T_{\text{inlet}} + \frac{Q_p}{c_w q} \tag{7}$$

A finite-element two-dimensional (2D) model to determine the temperature field in concrete blocks, including the cooling pipe system, was used. Segment No. 2 has the size of 0.75 × 1.4 (thickness by height). The type and dimensions of the investigated concrete wall are shown in Fig. 1. The pipe distance relative to the height of the concrete wall is 0.47 m, as shown in Fig. 2. The following parameters

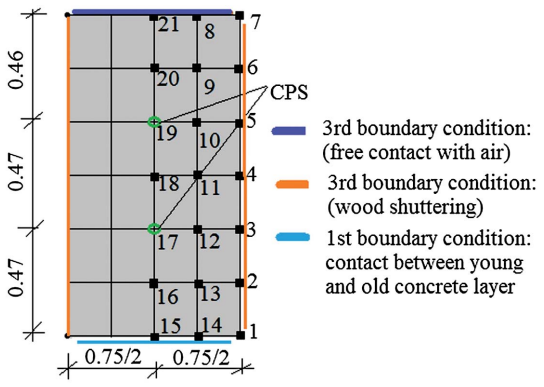

Fig. 2. Model geometry (meter).

of the CPS were assumed to perform the calculations: a heat transfer coefficient on the border with concrete of 381.20 $W/(m^2 \cdot ℃)$, a specific heat of 4,200 $J/(kg \cdot ℃)$, a coefficient of thermal conductivity of 0.64 $W/(m \cdot ℃)$, a water velocity in the pipe of 0.6 m/s, a water temperature in a pipe of 15℃, and a pipe diameter of 0.025 m.

The ambient temperature is assumed as follows:

$$T_{env} = 5℃ \sin\left(\frac{\pi \times t_{day}}{12}\right) + 15℃ \tag{8}$$

The temperature of the foundation slab under the concrete wall is assumed to be 15℃, and the initial temperature of the concrete mix when poured is assumed constant at 20℃. The mix proportion for segment No. 2 cement, CEM III A/42.5, was used.

The numerical model includes the equations in the advanced calculations of temperature changes of maturing concrete considering the effect of CPS. A similar approach but for a massive wall was validated, for example, by Azenha et al. (2014). However, the accuracy of a specific model mainly depends on the accuracy of the input data, which primarily relates to the thermomechanical properties of concrete in the considered case. The results of the material tests of concrete in this analysis and the construction of this structure were described by Zych (2015). The second important group of input data is external conditions, which are different for virtually every object in the crack analysis of maturing concrete due to the fluctuating ambient temperatures. In the comparative analysis of the variants without and with the CPS, Eq. (8) was used, which describes the change in ambient temperature. In the conditions of cyclically changing ambient temperature, Eq. (8) enables us to assess the effect of CPS on the analyzed structure. The actual temperature changes obtained from the analyses described by Zych (2008, 2011) were used to calculate the crack width according to Bamforth (2018), which enabled one to estimate the effect of CPS on the decrease in concrete cracking during its maturation. However, there is no experimental comparison of two identical structures simultaneously made with and without CPS, which would form the basis for inference based on the results of the in situ tests.

Mean Temperature Variations in Wall Section

To globally assess the effect of internal cooling, i.e., how it affects the entire section of the wall, temperature mean changes were determined for the entire section of the wall (Fig. 3). Fig. 3(a) shows the changes of the mean temperature relative to ΔT_{init}, while Fig. 3(b) shows those relative to T_{max}. The latter approach is commonly employed in engineering calculations [Eurocode 2 (CEN 2006)]. As follows from Fig. 3(a), in the variant with no internal cooling, the temperature decreases with a time delay, which will induce a higher increment of tensile stresses in the concrete with a slightly higher modulus of elasticity. Fig. 3(b) shows that the internal cooling presented in this form decreases the wall mean temperature change by as little as 2.36℃, but for the maximum value of −13.2℃, it increases by 18%. Consequently, internal cooling moderately reduces the mean temperature in the analyzed section of the wall. This effectiveness can be increased by designing a system of three cooling pipes. The mean temperature decrease in the wall section in the period of up to three days of concrete maturing with internal cooling is larger [Fig. 3(b)] than that with no internal cooling, which may result in the premature generation of tensile stresses in the young concrete in the case of more intensive cooling with the pipes.

Temperature Gradient

In the analysis of wall structures, the gradient along the wall height ΔT_{grad_y} is mainly considered. However, when the thermal boundary conditions on the wall vertical edges are highly diversified (e.g., the impact of solar radiation), it is reasonable to include the effect of the temperature gradient along the wall thickness ΔT_{grad_z}. The calculation of the temperature gradient ΔT_{grad_y} was based on the temperature changes in particular nodes of the wall and Eq. (9)

$$\Delta T_{grad\_y} = \frac{y}{I} \int_{-H/2}^{+H/2} b \times \Delta T_{mean\_y} \times y \times dy \tag{9}$$

where y = wall ordinate; ΔT_{mean_y} = mean temperature change in nodes at distance y away from neutral axis; and I = moment of inertia of the field temperature.

Detailed results are available in Appendix 1. Consequently, similar to the case of mean temperature variations $\Delta T_{mean}(t)$, internal cooling favorably affects the decrease in temperature gradient ΔT_{grad_y} along the vertical wall, which is important regarding the criterion of the cracking of walls in their lower parts. Moreover, similar to the distribution of the internal restraint rate, the temperature gradient ΔT_{grad_y} frequently determines the cracking range. Contributing to tensile strains on one of the edges, the temperature gradient induces opposite strains on an opposite edge. In practice, the temperature gradient ΔT_{grad_y} may determine the range of the zone in tension that requires more intensive reinforcement.

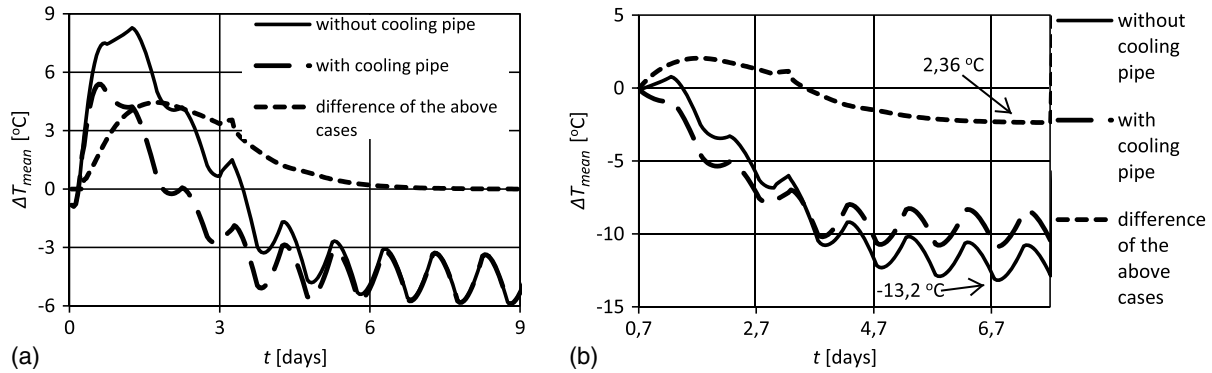

Fig. 3. Mean temperature differences $\Delta T_{mean}(t)$ for variants without and with CPS versus: (a) T_{init}; and (b) T_{max}.

Self-Equilibrating Temperature

The component of the temperature field, which is explicitly the least frequently included in engineering calculations and standard models, is temperature change $\Delta T_{eq}(y, z, t)$, which generates self-stresses (detailed results are available in Appendix 2). Appendix 2 clearly indicates that the employment of the CPS contributes to the overall decrease in a positive temperature difference in the areas of cooling pipes and their immediate vicinity. However, in these areas, negative temperature differences occur in the first four stages of concrete maturing, which generate compression-inducing strains in this part of the section. The positive temperature difference means that the difference between the temperature of the concrete (at the considered point of time) and the initial temperature of the concrete is positive. The negative temperature difference means that the aforementioned difference is negative. An unquestionable advantage of internal cooling is also a reduction of extreme values, i.e., positive values in the wall interior and negative ones in its corners. The comparison of the two last presented stages in the period of temperature stabilization, i.e., for $t = 3.83$ and 8.83 days [Figs. 8(i–l)], does not indicate any significant differences between them.

Self-Stresses

The application of the CPM after JSCE (2011) requires calculations that assume the average temperature variations along the wall thickness. In most cases, such calculations are sufficient for design purposes. However, to more precisely assess the quantitative impact of internal cooling in a semimassive wall while concrete is maturing, the self-stresses and their variations along both the height and thickness of the wall segment were also calculated (Appendix 3).

Total Self-Stresses

The self-stresses calculated in the presented method were summed with the stresses induced by the determined mean temperature variations and stress gradient. Fig. 4 illustrates the total stresses for the variant without the CPS on the outer wall edge, i.e., $z = -h/2$, and in the wall axis, i.e., $z = 0$. The diagrams show that the extreme compressive stresses of 2.0 MPa in the period of temperature increase occur in the midwall (i.e., for $y = 0.7$ m and $z = 0$), while near the wall surface (i.e., $y = 0.7$ m and $z = -h/2$), they are 1.26 MPa. The stresses that initiate cracking occur within four days of concrete maturing near the wall surface at half its height [Fig. 4(a)]. Cracking in the wall axis appears 24 h later and also at its half-height [Fig. 4(b)].

The comparison of the total stress variations without the CPS (Fig. 4) and those with the CPS (Fig. 5) shows that all values of stresses with the CPS are definitely lower. The tensile stresses exceed the tensile strength only in the midwall at its surface and in the wall axis only at 0.7 m. Therefore, the discontinuance of cooling after two days of concrete maturing and covering the wall with mats to protect it from fast heat transfer to the surroundings will probably prevent cracking.

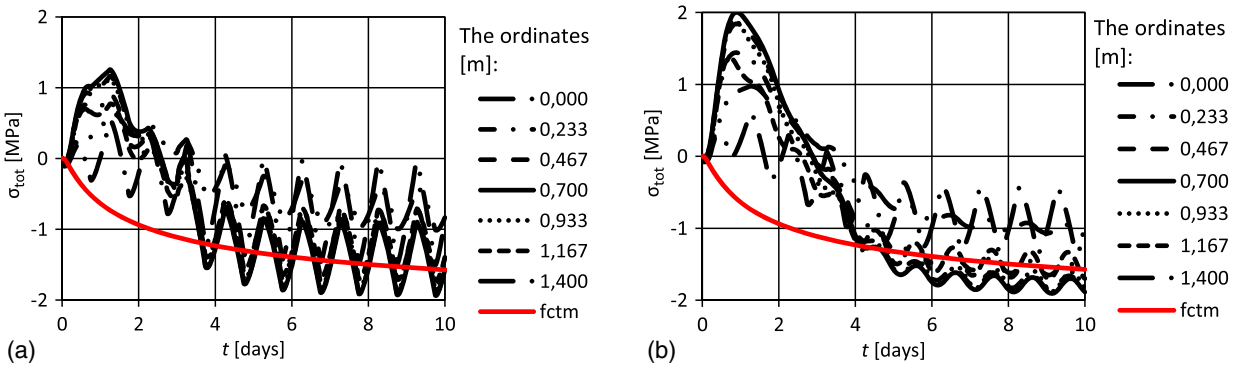

Fig. 4. Variations of total stresses for individual ordinates of segment No. 2 as a function of time for the variant without CPS: (a) on the outer edge; and (b) in the wall axis.

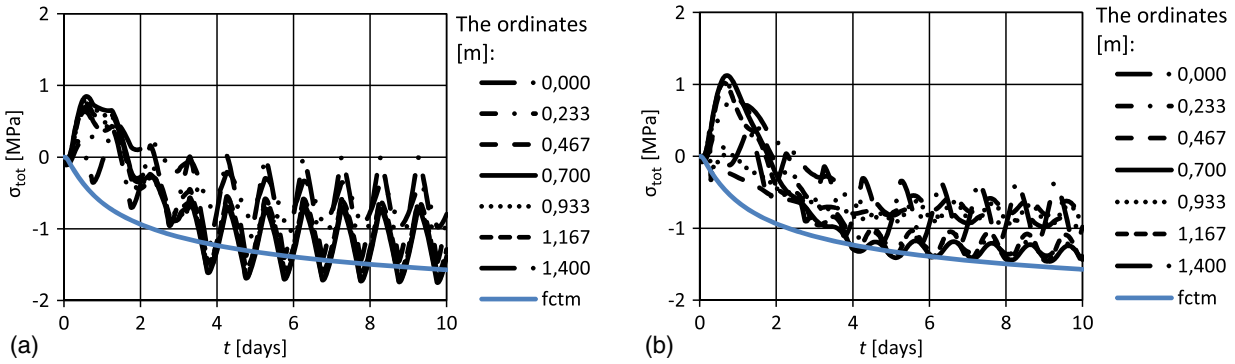

Fig. 5. Variations of total stresses for individual ordinates of segment No. 2 as a function of time for the variant with CPS: (a) on the outer edge; and (b) in the wall axis.

Table 3. Risk of early-age cracking of concrete

Ordinate y (m)	Cracking risk $r(t) = \sigma_{tot}(t)/f_{ctm}(t)$, for $t = 5.75$ days				Difference referring to variant without CPS (%)	
	Variant without CPS		Variant with CPS			
	Wall edge ($z = -h/2$)	Wall axis ($z = 0$)	Wall edge ($z = -h/2$)	Wall axis ($z = 0$)	Wall edge ($z = -h/2$)	Wall axis ($z = 0$)
0.000	0.62	0.59	0.64	0.60	+3	+2
0.233	1.24	0.98	1.18	0.86	−5	−12
0.467	1.34	1.11	1.22	0.43	−9	**−61**
0.700	1.35	1.14	1.24	0.87	−8	**−24**
0.933	1.30	1.08	1.19	0.47	−8	**−56**
1.167	1.19	0.96	1.13	0.83	−5	−14
1.400	1.03	0.91	1.02	0.88	−1	−3

Note: Bolded values indicate the most effective decrease in cracking risk.

Table 3 shows detailed data on the cracking risk defined as the $\sigma_{tot}(t)/f_{ctm}(t)$ ratio for time $t = 5.75$ days, i.e., when it has been exceeded in both solution variants. The risk values refer to both the outer edge and axis of the wall. In the last column, the differences in the percentage between the two variants are included. Due to the internal cooling, a decrease in the cracking risk is recorded in nearly the entire wall section, except the lower edge, where the risk slightly increases near the wall surface and its axis by 3% and 2%, respectively. The most effective decrease in a cracking risk of 61% was observed in the wall axis for ordinates $y \epsilon < 0.467\ \text{m} - 0.933\ \text{m} >$. Because the cracking risk in the variant without CPS is among the highest risks in this area, the intelligent use of internal cooling is an effective solution to prevent cracking in certain areas of a section. However, cracking first forms near the wall surface, where the cracking risk is reduced for $y = 0.7$ m, e.g., by only 8%. To better reduce the risk in the wall near-surface areas, cladding is recommended to insulate the wall surface against fast heat transfer to the surroundings.

The analysis of the cracking risk has shown that cracking also occurs in the variant with CPS. Moreover, it assesses and provides valuable information on the impact of internal cooling on the decrease in stresses and the cracking risk of maturing concrete in a semimassive wall.

Early Age and Long-Time Cracking According to CIRIA C766

The analysis of a semimassive structure in the period of concrete maturing contains the evaluation of its cracking risk and the prognosis of the possibility of limiting the crack width to the allowable value w_{lim}. The Bamforth (2018) guidelines define a method to calculate the width of cracks subjected to early-age and long-term imposed strains. The present analysis of cracking aims to compare the calculated crack widths with the values measured on a building site and evaluate the impact of internal cooling on limiting crack widths during concrete maturing and when long-term imposed strains are formed. Moreover, the analysis will help estimate the impact of internal cooling on the implementation of more economical solutions to reduce the necessary reinforcement amount to limit crack widths.

In the calculations of early-age cracking, the following quantities were adopted:

- Maximum temperature drop at an early age within a member $\Delta T_1 = 20.8$°C and 11.2°C for the variants without and with CPS, respectively;
- Autogenous shrinkage according to Eurocode 2 (CEN 2004), which is $\varepsilon_{ca} = 7\ \mu\varepsilon$ for $t = 3$ days;
- Maximum temperature difference between the wall interior and wall surface $\Delta T_{\max} = 6.1$°C and 4.3°C for the variants without and with CPS, respectively; and
- A restraint coefficient of imposed strains at the maximal crack width for an early age according to Bamforth (2018), which is $R_{ax} = 0.70$.

In the calculations of cracking for long-term imposed strains, the following quantities were adopted:

- Maximum temperature drop at an early age within a member $\Delta T_1 = 20.8$°C and 11.2°C for the variants without and with CPS, respectively;
- Autogenous shrinkage according to Eurocode 2 (CEN 2004), which is $\varepsilon_{ca} = 16\ \mu\varepsilon$ for $t = 28$ days;
- Drying shrinkage according to Eurocode 2 (CEN 2004), assuming completion of concrete curing after 2 days and shrinkage at 50 years ($\varepsilon_{cd} = 203\ \mu\varepsilon$);
- Long-term temperature change $\Delta T_2 = 25$°C (Zych 2011); and
- Restraint coefficient of imposed strains at maximum crack widths for long term according to Bamforth (2018), which is $R_{ax} = 0.65$.

Tables 4 and 5 show the values of restrained strains and cracking risks for early-age strains, early-age self-strains, and long-term strains, which are determined according to Bamforth (2018). The cracking risk at an early age induced by external restraints is not exceeded in the variant with the CPS and is 0.98. In the variant without the CPS, it is as high as 1.77. The cracking risk from early-age self-strains (0.30 and 0.21 in the variants without and with the CPS) should be summed up with the cracking risk that

Table 4. Restrained strains, cracking risks, and crack widths for early-age cracking

Cases	External restrained strains ($\mu\varepsilon$)		Self-strains ($\mu\varepsilon$)		Calculated crack width (mm)	
	Restrained strains $\varepsilon_{er\_e\text{-}a}$	Risk of cracking $\varepsilon_{r\_e\text{-}a}/\varepsilon_{ctu\_e\text{-}a}$[a]	Internal restrained strains $\varepsilon_{ir\_e\text{-}a}$	Risk of cracking $\varepsilon_{r\_e\text{-}a}/\varepsilon_{ctu\_e\text{-}a}$[a]	For outer surface of wall $w_{e\text{-}a,ext}$	For inner surface of wall $w_{e\text{-}a,int}$
Without CPS	98	1.77	17	0.30	0.03	0.04
With CPS	54	0.98	12	0.21	0.00	0.00

[a]$\varepsilon_{ctu\,e\text{-}a}$ = early-age tensile strain capacity = 55 $\mu\varepsilon$.

Table 5. Restrained strains, cracking risk, and crack widths in long-term cracking

Cases	External restrained strains ($\mu\varepsilon$)		Calculated crack width (mm)	
	Restrained strains $\varepsilon_{er\_e\text{-}a}$	Risk of cracking $\varepsilon_{r\_e\text{-}a}/\varepsilon_{ctu\_l\text{-}t}$ [a]	For outer surface of wall $w_{l\text{-}t,ext}$	For inner surface of wall $w_{l\text{-}t,int}$
Without CPS	273	2.65	0.10	0.14
With CPS	230	2.22	0.06	0.08

[a] $\varepsilon_{ctu\,l\text{-}t}$ = early-age tensile strain capacity = 103 $\mu\varepsilon$.

results from external restraints, i.e., the axial restraint of strains and restraint of the wall rotation. However, the analysis of stresses indicates that the maximum components of stresses and the level of cracking risk occur at different times. Therefore, it is reasonable to use cladding to help eliminate the extreme values of self-stresses. In the long-term case, the cracking risk is substantially higher for both variants and results from equally unfavorable external conditions. Hence, for the variants without and with CPS, it is 2.65 and 2.22, respectively. The calculated widths of the cracks at an early age for the variant without CPS for the outer and inner surfaces are 0.03 and 0.04 mm, respectively. The internal cooling eliminates the formation of cracks induced by external restraints.

After the period of concrete curing, semimassive walls of RC tanks are subject to further strains from ambient temperature variations and concrete shrinkage. In practice, it makes new cracks develop or widens the existing ones (Zych 2019). The calculated crack widths (Table 5) in long-term variants without the CPS on the inner and outer surfaces of a segment are 0.10 and 0.14 mm, respectively. The calculated crack widths on the wall surface that reached 0.2 mm should be compared with the long-term calculation results because the ambient temperature was merely −15°C at 13 days after wall concretion, as shown by Zych (2008). The calculated crack widths should be considerably underestimated due to the following:

- Extreme conditions due to ambient temperature variations when the given wall segment was executed; even before the concrete reached the 28-day strength, i.e., on the 13th day of concrete curing, the segment temperature dropped to 10°C (Zych 2008);
- Disregard of the impact of self-stresses on the surface cracks widths in the Bamforth (2018) model; and
- Locations of the measurements of crack widths 53 mm away from the reinforcement axis, while the calculations represent the crack mean width for the concrete effective zone in tension.

In the variant with the CPS, the widths of the calculated cracks on the segment outer and inner surfaces are 0.06 and 0.08 mm, respectively. All calculations were performed assuming that the coefficient of thermal expansion of concrete is $\alpha_T = 1.0 \times 10^{-5}$ 1/°C, i.e., the value recommended by Eurocode 2 (CEN 2004). In the absence of more precise data on the used concrete, Bamforth (2018) recommends a value higher by 20%: $\alpha_T = 1.2 \times 10^{-5}$ 1/°C.

These calculations show that internal cooling effectively helps to avoid cracking in the period of early-age concrete curing and limits the crack width in the long term. Due to internal cooling, the expected crack widths on both outer and inner surfaces of the wall are reduced by 40%.

Conclusions

The authors of the present paper did not participate in the construction of the structure in question. The proposed analytical study has resulted from their interests and experience, which were the basis for the proposal of a much more favorable structural solution to address the issue of early-age cracking in a new light. Based on the analysis of the impact of CPS on the changes in temperature, stresses, and crack width in an RC tank semimassive wall, both scientific conclusions that specify the directions of further research and practical conclusions for design engineers were formulated:

- Because the current state of knowledge concerns the use of a CPS in massive structures, the presented analysis of semimassive walls of RC tanks is an innovative approach to reduce or completely eliminate their early cracking. Therefore, further detailed conclusions are a novelty in semimassive structures.
- In RC semimassive tank walls, internal cooling reduces the changes in mean temperature, temperature gradient, and self-stress-inducing temperature. It also decreases the imposed strain restrained part, which causes tensile stresses and affects the watertightness of RC tank walls.
- In RC semimassive tank walls, the highest component of tensile stresses results from mean temperature variations of maturing concrete. The second highest is the component from self-stresses, while the lowest one is the stress gradient.
- It was demonstrated that internal cooling contributes to the decrease in the cracking risk of RC semimassive tank walls. Further research will enable one to determine the recommended period and rate of internal cooling to prevent cracking induced by excessive cooling, as shown in the analyzed example.
- The calculations of self-stresses for varying temperatures along the wall thickness show that internal cooling effectively decreases tensile stresses in the central part of the semimassive wall, particularly near the piping. Internal cooling is conducive

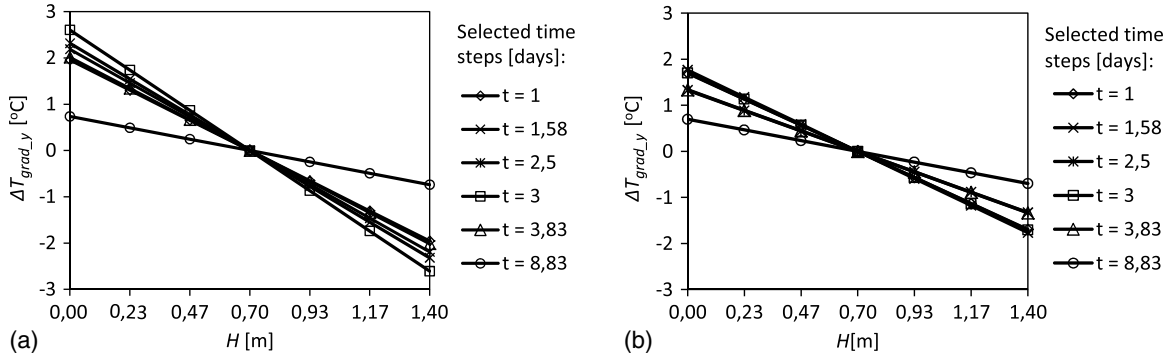

Fig. 6. Temperature gradients ΔT_{grad_y} at selected time points: (a) without CPS; and (b) with CPS (Appendix 1).

to the generation of favorable compressive stresses instead of tensile stresses.

- In RC semimassive tank walls, internal cooling moderately reduces the self-stresses in the near-surface areas, where cracking is usually initiated. Therefore, the cracking risks in these areas should be additionally reduced by the use of external cladding to prevent excessive heat transfer to the surroundings and more effectively reduce self-stresses.
- Following the current guidelines to calculate the crack width, it was demonstrated that the implementation of internal cooling in

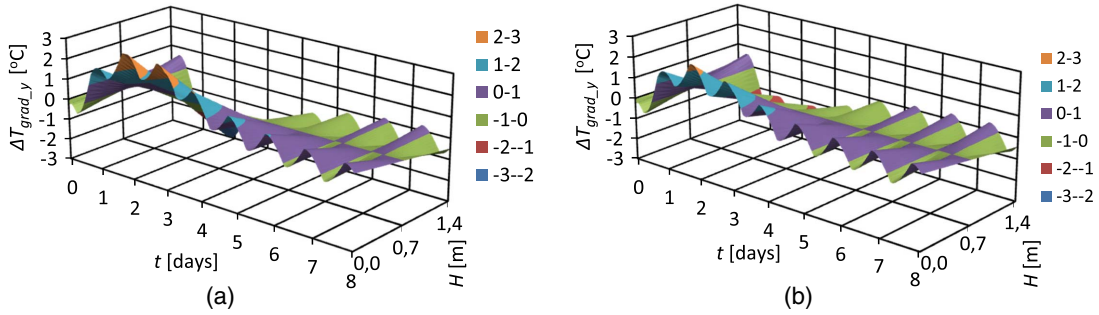

Fig. 7. Changes in temperature gradient $\Delta T_{\text{grad\_}y}$ in the vertical section of the wall: (a) without CPS; and (b) with CPS (Appendix 1).

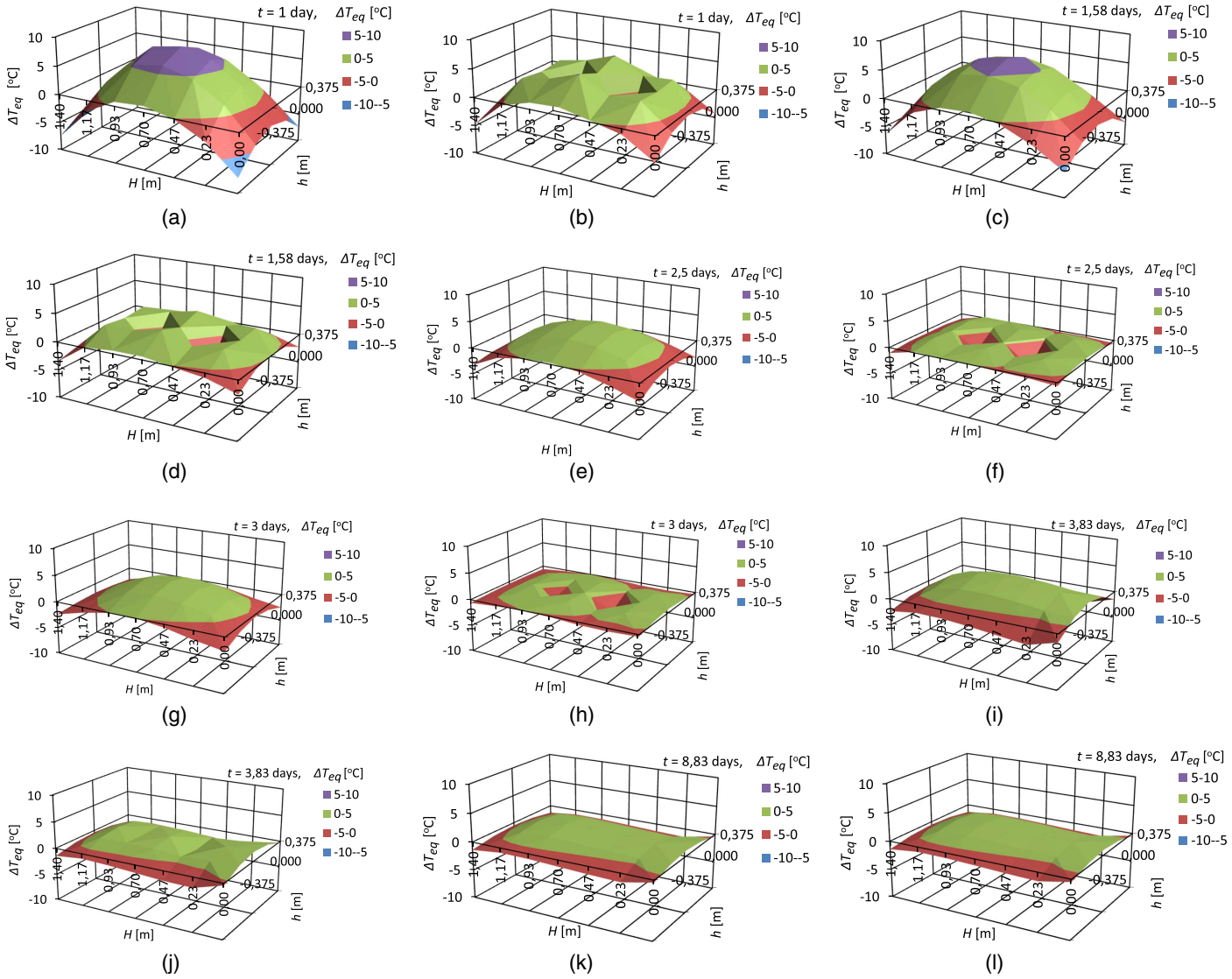

Fig. 8. Changes of temperature $\Delta T_{eq}(y,z)$ generating self-stresses for variants without and with CPS at subsequent points of time: (a) 1 day without CPS; (b) 1 day with CPS; (c) 1.58 days without CPS; (d) 1.58 days with CPS; (e) 2.5 days without CPS; (f) 2.5 days with CPS; (g) 3 days without CPS; (h) 3 days with CPS; (i) 3.83 days without CPS; (j) 3.83 days with CPS; (k) 8.83 days without CPS; and (l) 8.83 days with CPS (Appendix 2).

RC semimassive tank walls considerably reduces crack widths due to the cumulative impact of early-age and long-term imposed strains.

- The use of internal cooling in RC semimassive tank walls helps to economize on the necessary reinforcement quantity to reduce the imposed strain-induced crack widths.

Appendix 1. Temperature Gradient

Fig. 6 illustrates the temperature gradient $\Delta T\text{grad}\_y$ at selected time points for both calculation variants (i.e., without and with CPS).

In both cases, in the initial period of concrete maturing (i.e., temperature rise), the gradient will initiate minor tensile strains (due to lower temperature) on the wall upper edge and compressive strains (due to higher temperature) on the bottom edge of the wall [Figs. 7(a and b)].

In general, it can be stated that in neither calculation variant is the temperature gradient high, but owing to internal cooling, for instance, $t = 3$ days, ΔT_{grad_y} is lower by 35%. The favorable effect of internal cooling on temperature gradient reduction can be accounted for by the location of cooling pipes, which reduces the temperature within the wall more effectively than near its surface, also contributing to the mitigation of temperature differences at the opposite edges of the wall.

Appendix 2. Self-Equilibrating Temperature

In Fig. 8, temperature changes $\Delta T_{eq}(y, z, t)$ are presented (description in the paper).

Appendix 3. Self-Stresses

Fig. 9 illustrates self-stresses variations for selected time steps in the variants without and with CPS. What is notable is that initially, i.e., until $t = 1.58$ days, internal cooling reduces both the compressive stresses in the midwall and the tensile stresses in the wall corners very effectively [cross reference Figs. 9(a) with 9(b) and

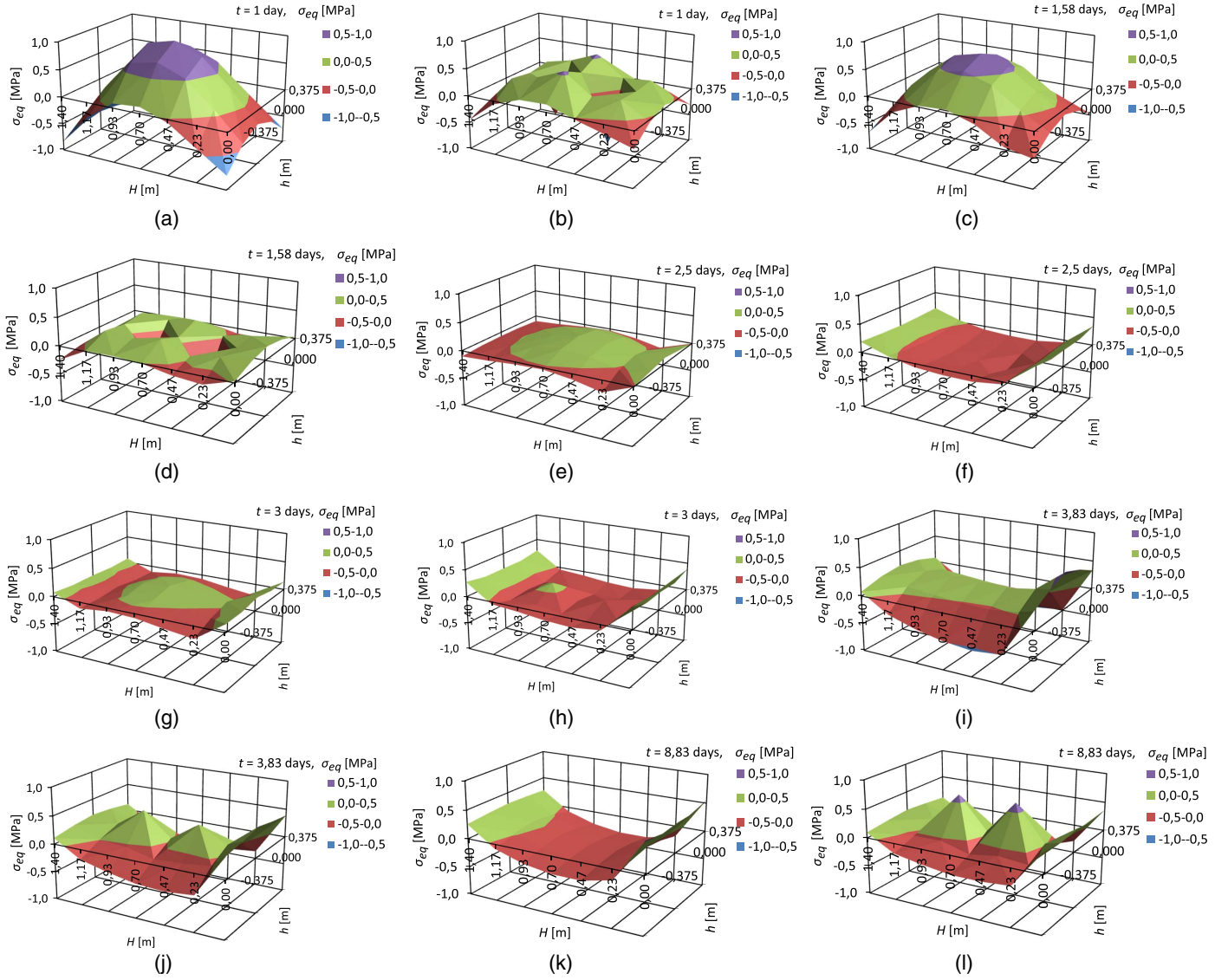

Fig. 9. Self-stresses $\sigma_{eq}(y, z)$ for variants without and with CPS for subsequent points in time: (a) 1 day without CPS; (b) 1 day with CPS; (c) 1.58 days without CPS; (d) 1.58 days with CPS; (e) 2.5 days without CPS; (f) 2.5 days with CPS; (g) 3 days without CPS; (h) 3 days with CPS; (i) 3.83 days without CPS; (j) 3.83 days with CPS; (k) 8.83 days without CPS; and (l) 8.83 days with CPS. (Appendix 3).

Figs. 9(c) with 9(d)]. In the subsequent time steps, i.e., $t = 2.5$ and 3 days [cross reference Figs. 9(e) with 9(f) and Figs. 9(g) with 9(h)], the distribution of extreme values of self-stresses in the entire section is comparable. In the variant with CPS, on the other hand, in the final cooling stage, i.e., for $t > 3.83$ days [Figs. 9(j and l)], definitely greater compressive stresses prevail in the midwall (over 0.5 MPa) compared with variants without the CPS [Figs. 9(i and k)] in which the stresses are tensile and are up to −0.5 MPa.

Data Availability Statement

All data, models, and code generated or used during the study appear in the published article.

References

Aleksandrovski, S. V. 1966. *Calculations of concrete and reinforced concrete structures subjected to temperature and humidity changes (including creep)*. Moskwa: Strojizdat.

Azenha, M., R. Lameiras, C. de Sousa, and J. Barros. 2014. "Application of air cooled pipes for reduction of early age cracking risk in a massive RC wall." *Eng. Struct.* 62–63 (Mar): 148–163. https://doi.org/10.1016/j.engstruct.2014.01.018.

Bamforth, P. B. 2018. *Control of cracking caused by restrained deformation in concrete*. London: Construction Industry Research and Information Association.

Bofang, Z. 2014. *Thermal stresses and temperature control of mass concrete*. Oxford, UK: Butterworth-Heinemann.

CEN (European Committee for Standardization). 2004. *Design of concrete structures: General rules and rules for buildings, part 1.1*. Eurocode 2. Brussels, Belgium: CEN.

CEN (European Committee for Standardization). 2006. *Design of concrete structures: Liquid retaining and containment structures, part 3*. Eurocode 2. Brussels, Belgium: CEN.

Chen, S., P. Su, and I. Shahrour. 2011. "Composite element algorithm for the thermal analysis of mass concrete." *Int. J. Numer. Methods Heat Fluid Flow* 21 (4): 434–447. https://doi.org/10.1108/09615531111123100.

Fairbairn, E. M. R., and M. Azenha. 2019. *Thermal cracking of massive concrete structures. State-of-the-art report of the RILEM Technical Committee 254-CMS*. New York: Springer.

Flaga, K. 2004. *Shrinkage stress and reinforcement in concrete structure. Monograph 295*. Cracow, Poland: Cracow Univ. of Technology.

Hamfler, H. 1988. *Berechnung von Temperatur-, Feuchte- und Verschiebungsfeldern in erhärtenden Betonbauteilen nach der Methode der Finite Elemente" [Calculation of temperature, humidity and displacement in hardening concrete elements using the finite element method].* [In German.] Hannover, Germany: Institut für Massivbau.

Hauser, G., C. Kempkes, and B. W. Olesen. 2000. "Computer simulation of hydronic heating/cooling system with embedded pipes." In *Proc., ASHRAE Winter Meeting, American Society of Heating, Refrigerating and Air Conditioning Engineers*, 702–710. Dallas: American Society of Heating, Refrigerating and Air Conditioning Engineers.

Hong, Y. X., W. Chen, J. Lin, and J. Gong. 2017. "Thermal field in water pipe cooling concrete hydrostructures simulated with singular boundary method." *Water Sci. Eng.* 10 (2): 107–114. https://doi.org/10.1016/j.wse.2017.06.004.

Jędrzejewska, A., F. Kanavaris, M. Zych, D. Schlicke, and M. Azenha. 2020. "Experiences on early age cracking of wall-on-slab concrete structures." In Vol. 27 of *Structures*, 2520–2549. London: Elsevier. https://doi.org/10.1016/j.istruc.2020.06.013.

JSCE (Japan Society of Civil Engineers). 2011. *Guidelines for concrete. No. 15: Standard specifications for concrete structures. Design*. Tokyo, Japan: JSCE.

Kanavaris, F., et al. 2021. "Enhanced massivity index based on evidence from case studies: Towards a robust pre-design assessment of early-age thermal cracking risk and practical recommendations." *Constr. Build. Mater.* 271 (Feb): 121570. https://doi.org/10.1016/j.conbuildmat.2020.121570.

Knoppik-Wróbel, A. 2015. "Analysis of early-age thermal-shrinkage stresses in reinforced concrete walls." Ph.D. thesis, Faculty of Civil Engineering, Silesian Univ. of Technology.

Kogan, E. A. 1980. "Stress relaxation in concrete of massive hydraulic structures." *Hydrotech. Constr.* 14 (9): 916–920. https://doi.org/10.1007/BF02305447.

Li, C., and Y. Li. 2017. "Optimization of cooling pipes inside mass concrete bridge pile cap." In *Proc., 2nd World Conf. on Humanities and Social Sciences (WCHSS)*, 25–30. London: Francis Academic Press.

Liu, X., C. Zhang, X. Chang, W. Zhou, Y. Cheng, and Y. Duan. 2015. "Precise simulation analysis of the thermal field in mass concrete with a pipe water cooling system." *Appl. Therm. Eng.* 78 (5): 449–459. https://doi.org/10.1016/j.applthermaleng.2014.12.050.

Myers, T. G., N. D. Fowkes, and Y. Ballim. 2009. "Modeling the cooling of concrete by piped water." *J. Eng. Mech.* 135 (12): 1375–1383. https://doi.org/10.1061/(ASCE)EM.1943-7889.0000046.

Nguyen, C. T., and N. A. Aniskin. 2019. "Temperature regime during the construction massive concrete with pipe cooling." *Mag. Civ. Eng.* 89 (5): 156–166. https://doi.org/10.18720/MCE.89.13.

Nguyen, T.-C., T. P. Huynh, and V. L. Tang. 2019. "Prevention of crack formation in massive concrete at an early age by cooling pipe system." *Asian J. Civ. Eng.* 20 (8): 1101–1107. https://doi.org/10.1007/s42107-019-00175-5.

Qiu, Y., and G. Zhang. 2017. "Stress and damage in concrete induced by pipe cooling at mesoscopic scale." *Adv. Mech. Eng.* 9 (2): 1–17. https://doi.org/10.1177/1687814017690509.

Rostásy, F. S., and M. Krauß. 2003. *Frühe Risse in massigen Betonbauteilen—Ingenieurmodelle für die Planung von Gegenmaßnahmen" [Early cracks in massive concrete elements—Engineering models for planning countermeasures].* [In German.] Berlin: Beton- und Stahlbetonbau, Ernst & Sohn. https://doi.org/10.1002/best.200301130.

Seruga, A., and M. Zych. 2015. "Thermal cracking of the cylindrical tank under construction. I: Case study." *J. Perform. Constr. Facil.* 29 (4): 04014100. https://doi.org/10.1061/(ASCE)CF.1943-5509.0000581.

Van Breugel, K. 1996. *Betonconstructies onder Temperatuur-en Krimpvervormingen—Theorie en Praktijk*. Delft, Netherlands: TU Delft.

Voigt, T. 1994. *"Frosteinwirkung auf mineralische Deponieabdichtungen" Heft 47 [Impact of frost on the tightness of the mineral landfills].* [In German.] Berlin: Diss TU Braunschweig.

Zych, M. 2008. "Numerical analysis of cracking in hardening concrete of RC tank's wall." *Tech. Trans.* 20 (105): 227–249.

Zych, M. 2011. "Analysis of RC tank's walls during early hardening period of concrete." Ph.D. thesis, Division of Structural Engineering, Cracow Univ. of Technology.

Zych, M. 2015. "Case study of concrete mechanical properties development based on heat temperature measurements." *Cem. Lime Concr.* 6: 383–392.

Zych, M. 2019. "A new model for crack control in reinforced concrete tank walls—Part I: Analytical investigation." *ACI Struct. J.* 116 (3): 85–94. https://doi.org/10.14359/51713317.